Impact of boronizations on impurity sources and performance in Wendelstein 7-X

S. Sereda[1], S. Brezinsek[1], E. Wang[1], T. Barbui[2], R. Brakel[3], B. Buttenschön[3], A. Goriaev[4,5], U. Hergenhahn[3], U. Höfel[3], M. Jakubowski[3], A. Knieps[1], R. König[3], M. Krychowiak[3], S. Kwak[3], Y. Liang[1], D. Naujoks[3], A. Pavone[3], M. Rasinski[1], L. Rudischhauser[3], M. Ślęczka[6], J. Svensson[3], H. Viebke[3], T. Wauters[4], Y. Wei[7], V. Winters[3], D. Zhang[3] and the W7-X Team[3]

[1)]Forschungszentrum Jülich GmbH, Institut für Energie- und Klimaforschung – Plasmaphysik, Partner of the Trilateral Euregio Cluster (TEC), Jülich, Germany
[(2)]Princeton Plasma Physics Laboratory, Princeton, United States of America
[(3)]Max-Planck-Institut für Plasmaphysik, Greifswald, Germany
[(4)]Laboratory for Plasma Physics, LPP-ERM/KMS, Brussels, Belgium, Trilateral Euregio Cluster (TEC) Partner
[(5)]Department of Applied Physics, Ghent University, Belgium
[(6)]University of Szczecin, Szczecin, Poland
[(7)]Southwestern Institute of Physics, Chengdu, People's Republic of China

Abstract

The low-Z oxygen and carbon were the main plasma impurities in the Wendelstein 7-X (W7-X) stellarator in the last experimental campaign with the passively cooled graphite divertor. To tackle this issue boronization [1] was applied, which has led to one of the main achievements of the campaign: plasma operation at high core densities of more than 10^{20} m^{-3} in hydrogen fueled plasmas due to the reduced radiation-induced density limit.
In total three boronizations were applied. After the first boronization the oxygen to hydrogen flux ratio (normalized influx of oxygen) at the divertor substantially decreased by a factor of 10 and the carbon to hydrogen flux ratio (normalized influx of carbon) decreased by a factor of 4 as obtained from spectroscopy. In the same time, boron emission appeared in the spectra. Between the boronizations oxygen and carbon normalized influxes increased but never reached the pre-boronization values. With each subsequent boronization O level decreased even more, reaching the lowest values after the third boronization which were more than a factor of 100 lower than before the first boronization.
Such a decrease in low-Z impurity concentration significantly extended the operation window of W7-X in terms of line-integrated electron density (from $4 \cdot 10^{19}$ m^{-2} to more than $1 \cdot 10^{20}$ m^{-2}) and diamagnetic energy (from 330 kJ up to 510 kJ). Z_{eff} decreased from 4.5 down to values close to 1.2 as obtained from bremsstrahlung measurements. The above mentioned values are given for the two reference discharges before and after boronization.

1. Introduction

The low-Z elements oxygen and carbon were the main plasma impurities during the last operational phase OP1.2 at Wendelstein 7-X stellarator. Carbon was an intrinsic impurity because of the wall material and oxygen was an intrinsic impurity due to contamination of the plasma vessel. During OP1.2 campaign the device was equipped with the test divertor unit (TDU) made of fine grain graphite which was inertially cooled [2]. The TDU was the most heavily loaded plasma-facing component (PFC) since W7-X uses an island divertor concept [3]. In this concept a chain of intrinsically present magnetic islands exists outside of the last closed magnetic surface for effective particle and energy exhaust. The magnetic field lines of these islands are cut by the divertor targets of TDU and most of the plasma-surface interaction (PSI) takes place at this strike line area.

Both divertor and core spectroscopy showed a presence of strong lines of neutral atoms and ions of low-Z O and C species during a plasma discharge. In addition, mass spectrometry showed high levels of H_2O, CO and CO_2 during and after a plasma discharge. Such a problem is known for plasma devices with carbon divertors and stainless steel walls [4,5-6]. Oxygen is present on the stainless steel walls in the form of metal oxides. During a plasma discharge it interacts with hydrogen and is desorbed from the surface as water, which is subsequently ionized, dissociated and confined in the plasma. Eventually, O is transported to the C divertor and chemically reacts with C producing CO and CO_2 molecules [7].

The large surface area of the graphite divertor also served as a reservoir for water. During an experimental day water levels would increase, as shown by mass spectrometry in Figure 1, due to the increase of divertor target temperature with every discharge. This

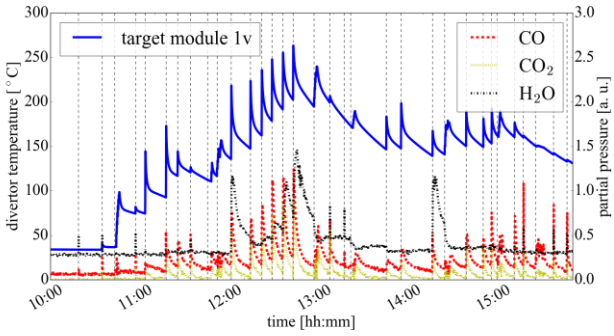

Figure 1: Temperature of the divertor module 1v (close to the strike line location) of the upper divertor target M51 of W7-X (left axis) and partial pressure of CO, CO_2 and H_2O (right axis) on the last day before boronization: 20180801.

caused water to come out from the graphite target and participate in the cycle described above. The picture is analogous to the first experimental phase with TDU [8].

In addition, other processes contributed to C erosion. Those are physical sputtering by energetic protons, O and C ions. Chemical erosion of C by H also plays an important role. Mass spectrometry showed CH_4 production in the machine before and after boronization [9]. In contrast, no signs of chemical erosion by H had been detected by local optical spectroscopy measurements at the divertor target before boronization and shortly after as suggested by the 425-430 nm range, where no CH Gerö band [10] was detected. This is a sign that chemical erosion of C by H plays less important role than physical sputtering of C at the divertor target.

As W7-X is aiming for steady-state operation for 1800 s with high core plasma parameters in the future, the control of impurities influx and oxygen content is necessary. In addition, the lifetime of the main PFCs is an important question in this case. Minimal erosion of highly loaded graphite components is required.

Plasma assisted cleaning techniques, such as glow discharge cleaning in helium and hydrogen (He-GDC and H-GDC), electron-cyclotron wall conditioning (ECWC) in helium were used as the standard method of wall conditioning techniques. Nevertheless, H_2O was reappearing after subsequent plasma discharges due to desorption from the metal walls [9].

Taking into account the above considerations another very effective method of wall conditioning was applied – covering of the plasma-facing components with a protective layer of low-Z material. In this case the boronization was chosen – plasma-chemical in-situ deposition of a protective boron layer on all plasma-facing components. It was pioneered on TEXTOR [1] and then successfully applied in different devices like W7-AS [4], ASDEX [11], LHD [12], Tore Supra [13], DIIID [14] and other devices.

The boronization was performed in a He-GDC with 90% He and 10% B_2H_6. This procedure was conducted 3 times with 45, 84 and 68 bar*l of He-B_2H_6 mixture. Durations of the boronizations were 3.5, 5.5 and 5 hours correspondingly. Boronization caused a substantial reduction in O as well as in CO and CO_2. C levels were decreased too.

Section 2 explains the experimental approach used to characterize boronization. Section 3 is devoted to the line emission reduction and explaining the device performance improvement. Section 4 is focused on short time and long-time effects of boronizations on impurity concentration. In section 5 results of a post-mortem analysis of the divertor are discussed to elaborate more on the mechanism of boronizations and it is followed by the summary and the discussion.

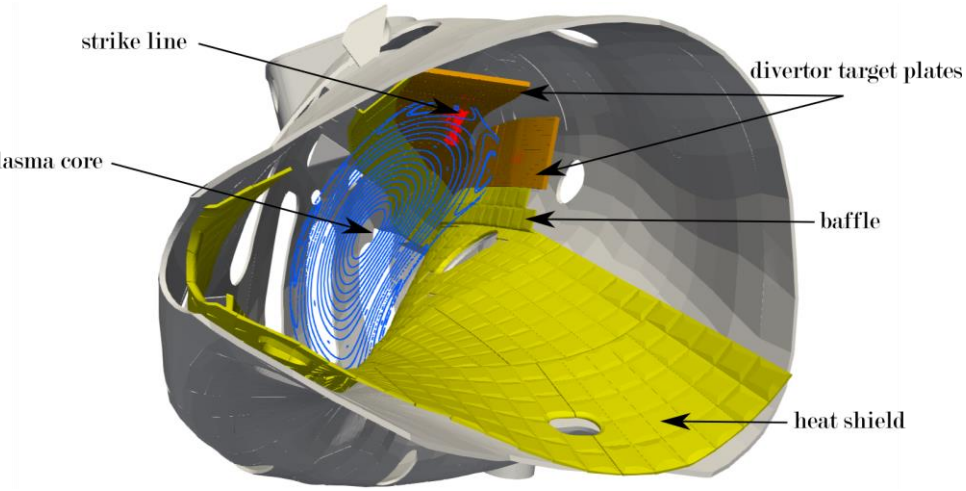

Figure 2: Plasma-facing components of Wendelstein 7-X

2. Experimental approach

In order to study the effects of boronizations, a dedicated set of plasma discharges has been performed on W7-X. The most relevant experimental program was the very last day before the first boronization and the first day after it. Two types of reference discharges were performed on each day:

1. "Power steps" – density of the plasma was kept constant during a discharge, electron cyclotron resonance heating (ECRH) power (P_{ECRH}) was increased in steps of 1 MW. These discharges were used to study impurity levels and composition of plasma.

2. "Density ramps" – ECRH heating power was kept constant and the plasma density was raised gradually until plasma collapse caused by the radiation-induced density limit [15].

The first boronization assessment was performed in the standard magnetic configuration of W7-X. The subsequent boronizations were preceded or followed by plasma discharges in different magnetic configurations and are not considered in this paper.

After the initial study of the boronization the "power steps" reference discharge was repeated regularly as the first discharge of an experimental day. In contrast to the initial experimental program, in this case the magnetic configuration was depending on the experimental program of the day.

The relation between impurity levels and total plasma exposure time of the PFCs is important to understand possible outcomes for future operational campaigns. Therefore, a full set of encompassing plasma duration in each discharge is required. Such statistics were obtained for all discharges and diamagnetic energy threshold of the plasma W_{dia}>50 kJ was used as criterion of plasma in the device. If W_{dia} data was not available then P_{ECRH} > 0.05 MW condition was taken. The results are summarized in Table 1. The corresponding distribution of the heat flux on the divertor targets of W7-X in different magnetic configurations is shown in Figure 3.

In order to study the effects of boronizations on PSI processes the PFCs of W7-X can be divided into 2 groups (see Figure 2):

1. Main PFCs – fine-grain graphite divertor, were most of the PSI takes place.

2. Recessed PFCs – stainless steel vessel wall, carbon heat shield and carbon baffle.

It was expected that at the main PFCs boron would be quickly eroded by ions. Simultaneously, the carbon levels would quickly reappear. For the remote PFCs erosion processes for boron would be one order of magnitude slower, but still taking place due to the erosion by charge exchange neutrals and residual ions.

Table 1: Statistics of the plasma exposure time for the OP1.2b experimental campaign of W7-X

Configuration family	Number of discharges	Plasma time [s]	Fraction of time [%]
Standard	638	4809	53.1
High-mirror	234	1392	15.3
Low-iota	169	1180	13.0
High-iota	315	1673	18.5
Total	1256	9054	-

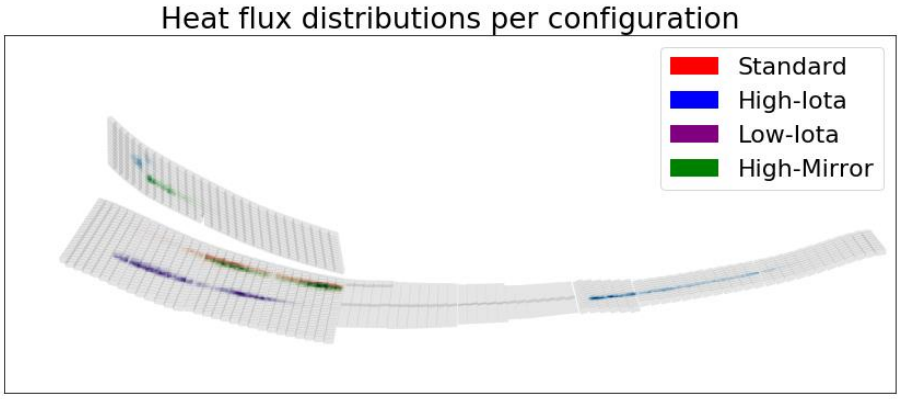

Figure 3: Expected heat-flux distributions derived by vacuum field-line diffusion modelling for the four main configurations of W7-X. Colours indicate configuration and opacity represents the normalized heat-load

The overview spectrometer system [16] was used as the main tool to characterize the effects of boronizations on impurity sources at the main PFCs. In this case the overview spectrometer was connected to the endoscope at the AEJ51 port [17, 18] of W7-X at the toroidal angle $\varphi = 302.9^{o}$. It allowed observation of line emissions in a wide range from 350 nm to 1050 nm with frequencies of 1 – 10 Hz depending on plasma emission intensity. The field of view of the overview spectrometer for the standard magnetic configuration of W7-X is shown in Figure 4. It allows obtaining photon flux from the divertor target including strike-line location.

A set of Langmuir probes is located at the surface of the divertor target close to the strike line location [19]. It allows electron temperature T_e and electron density n_e measurements in the vicinity of the highest photon flux coming from B, C, O and H. Its location is shown in Figure 4 in yellow dots.

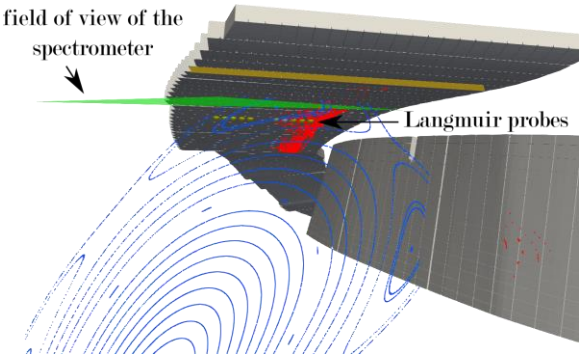

Figure 4: Field of view of the overview spectrometer (green) for the standard magnetic configuration of W7-X. The strike-line location is shown only for the magnetic island in the field of view (red, "vacuum" case). The Poincaré map is depicted in blue. Positions of the TDU Langmuir probes are shown in yellow dots. Horizontal and vertical divertor target plates are shown in grey.

Impurity sources at remote PFCs were monitored with the filterscope system [20]. There were 2 fields of view looking at the graphite shield and the stainless steel wall. The former one allowed observation of CIII (C^{2+}, 465.4 nm) and OII (O^{+}, 441.9 nm) line emission and the latter one CIII only. These are shown in Figure 5.

Assuming ionizing plasma conditions the particle flux can be obtained from the photon flux of the specific electron transition in an ion or a neutral. The proportionality coefficient gives the number of ionizations per photon and is typically denoted S/XB. Ionization conditions were the case in the last experimental campaign for all discharges with attached scenarios.

Therefore, by knowing corresponding S/XB coefficients, for example from [21], local T_e and n_e, it is possible to obtain particle fluxes from the measured photon fluxes. The CII flux was shown to be representative for the total carbon erosion [22]. The OI, BII lines can be used to deduce oxygen and boron levels. The H_γ line represents total H recycling flux.

The other important diagnostics is HEXOS: High-Efficiency XUV Overview Spectrometer, since its field of view goes through the core of the plasma. Taking into account its wavelength range of 3-160 nm higher ionization stages of impurities can be detected in the main plasma.

f_{rad} - fraction of radiated power (ratio between the total radiated power to the total ECRH heating) was measured by the bolometry system [23].

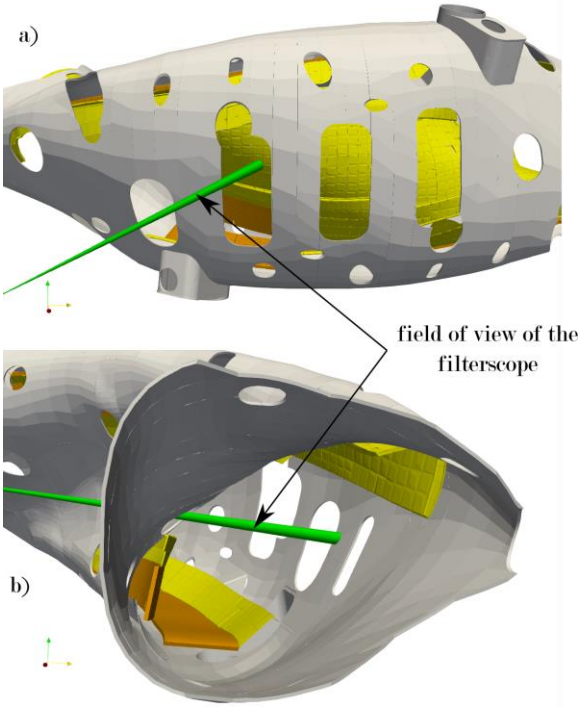

Figure 5: Field of view of the used line of sight of the filterscope system at: a) AEK10 port (toroidal angle φ = [-4.8, -10.1°]) looking at the carbon shield and at b) AEL30 port (φ = [126.5°, 130.8°]) looking at the stainless steel wall.

After the boronization plasma conditions significantly changed and were dependent on the specific discharge. Therefore, line radiation from higher ionization stages of B (BV 4.9 nm by B^{4+}), C (CVI 3.4 nm by C^{5+}), O (OVI 13 nm by O^{5+}) was normalized to the line integrated electron density and was representative for their concentration in the main plasma. The impurity fluxes at the divertor were normalized to the hydrogen flux to represent their normalized influx from the divertor target.

3. Performance improvement of the device

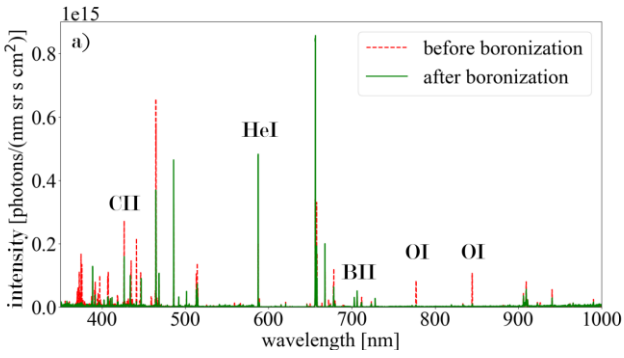

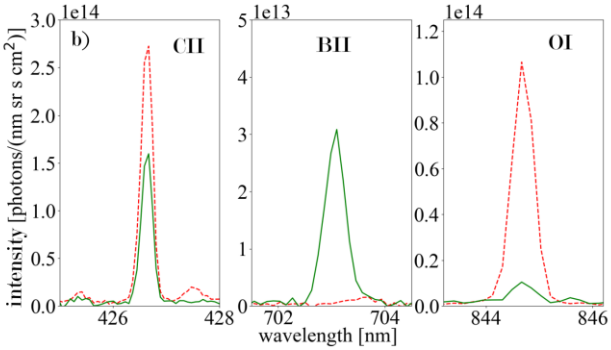

Figure 6: Emission spectra measured at the divertor before (red, discharge 20180801.021) and after (green, discharge 20180807.011) the first boronization of W7-X a) in the range of 350 nm – 1000 nm and b) in the vicinity of CII, BII and OI lines.

After the first boronization a substantial reduction of the line radiation of O and C was observed. In Figure 6 an emission spectrum is shown for the reference discharges before the first boronization (20180801.021), and after the first boronization (20180807.011) with similar conditions. For both discharges a moment at the flat top with heating power P_{ECRH} = 3 MW and line integrated density approximately $2 \cdot 10^{19}$ m^{-2} has been selected. From Figure 6 it is clear that the most intensive OI (atomic oxygen) lines at 777.2 nm and 844.7 nm have substantially decreased. The intensity of the CII (C^{1+}) line at 426.7 nm has also significantly decreased. The newly arisen BII line at 703.1 nm is emitted by B^{+}. No detectable signs of the molecular CH Gerö band with the head at 430 nm were found on the last day before and the first day after the first boronization.
The same qualitative behaviour is observed in the XUV spectrum obtained by core spectroscopy. The line radiation of O dropped significantly, the C emission decreased and a newly arisen B was seen, as expected, in the spectra (Figure 7).

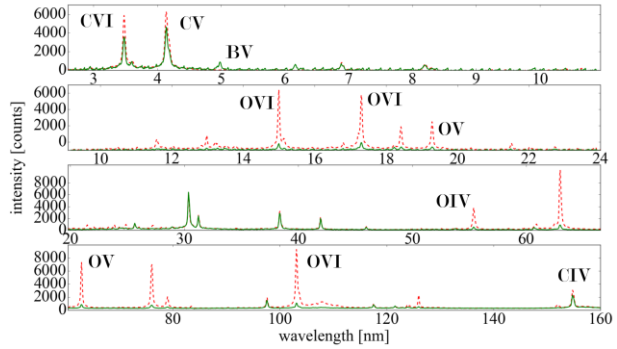

Figure 7: Emission spectra in the range 2.6 – 160 nm obtained with HEXOS before (red dashed) and after

(green) the first boronization. The corresponding discharges are as in Figure 6.

Due to substantially decreased line radiation of low-Z impurities O and C the operational window of W7-X was significantly widened in terms of maximum plasma density and stored energy.

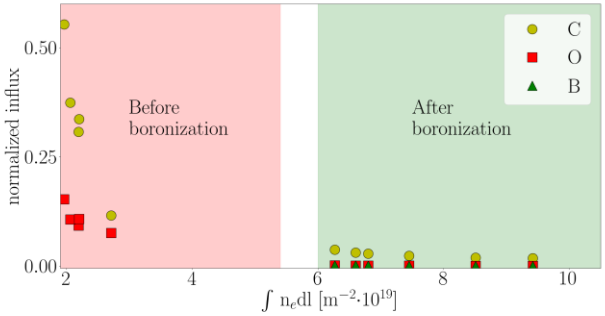

Figure 8: Normalized influx of low-Z O and C together with introduced B. Two discharges are shown on the plot: 20180801.036 before the first boronization (red background) and 20180807.013 after (green background).

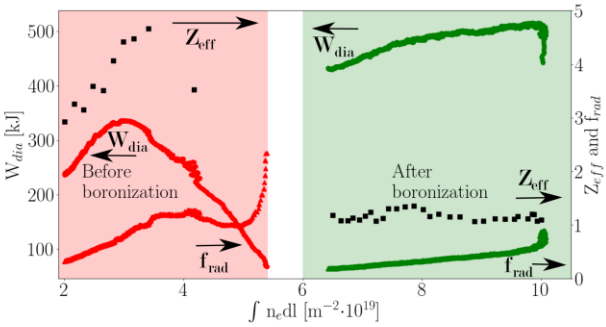

Figure 9: Diamagnetic energy, Z_{eff} and radiation fraction of the plasma as a function of the line integrated electron density before boronization (red, 20180801.036) and after (green, 20180807.013) boronization.

Figure 8 shows two dedicated discharges of a 'density ramp' type before and after the first boronization. Impurity normalized influx of O and C is shown before and after boronization and newly arisen B is present after it. The first boronization resulted in much higher densities. Before it was possible to get line-integrated electron densities up to $4 \cdot 10^{19}$ m^{-2} and after values of $1.1 \cdot 10^{20}$ m^{-2} were achieved. Before boronization the electron density profiles were flat [24]. Therefore, having value of the electron line-integrated density together with the length of integration ~1.33 m the line-averaged electron density can be easily calculated, which is well representing the core electron density. After boronization the electron density profile has obtained slight picking in the core of the plasma which is ~30% higher than the line-averaged value. This results in the core electron densities reaching 10^{20} m^{-3} after boronization. Simultaneously, impurity normalized influx of O and C dropped approximately by a factor of 4 for C and by approximately a factor of 50 for O right after the first boronization. One should keep in mind that the density after boronization significantly increased and the values in this case can not be compared directly.

Such a reduction in impurities normalized influx resulted in increased line-integrated electron density. This increase also allowed diamagnetic energy of the plasma to increase from approx. 330 kJ up to approx. 510 kJ after boronization (see Figure 9). The fraction of radiated power f_{rad} has decreased too. It is known that the impurity concentration decrease leads to the increased critical density $\sim f_{imp}^{-\beta}$ [24]. Radiation power is mainly following the line radiation of oxygen [25]. In addition, values of Z_{eff} obtained from bremssrahlung radiation decreased from values of around 4.5 for all densities down to low values of around 1.2.

4. Short and long-time effect of boronizations

Both short and long-time effect of boronization study is needed to understand the mechanisms of impurity reduction and predict the necessity of further boronizations. The normalized influx of B and C at the strike line are shown in Figure 10a. Apparently, B is quickly eroded there until a rather constant low level due to balance between its erosion and re-deposition. This happens after the 59 s of plasma exposure time (15 discharges) after boronization. Simultaneously, C behaves in the same way. The ratio between C and B fluxes (Figure 10b) increases with every discharge and together with Figure 10a it shows quick erosion of B and increase of C levels. Oxygen behaviour is not shown here since its line radiation wasn't detectable with the overview spectrometer during the first discharges after boronization.

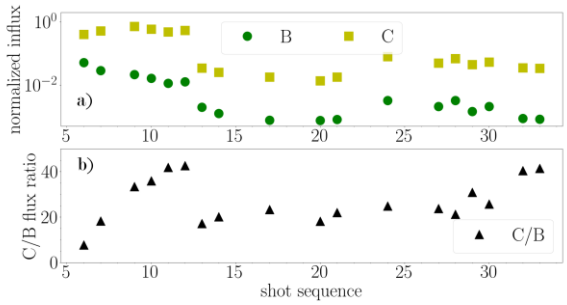

Figure 10: a) B and C normalized influx as a function of a discharge number on the first day after

boronization. b) Ratio of C to B fluxes for the same operational day of W7-X. Standard magnetic configuration.

The temporal evolution of B, C and O normalized influx at the divertor and their concentration in the main plasma over the complete experimental campaign are shown in Figure 11a and 11b correspondingly. Right after the first boronization O normalized influx at the divertor substantially decreased ~ by a factor of 10. In contrast, the C yield dropped by a factor of 4. After 1000 s of plasma exposure time in different magnetic configurations O and C normalized influx didn't show a significant increase. In contrast, B eroded rather quickly at the strike line location and divertor. The average values obtained with the Langmuir probe were $T_e \sim 51$ eV and $n_e \sim 6.8 \cdot 10^{18}$ m^{-3} for the discharges used in Figure 11a. With the second and the third boronizations O normalized influx at the divertor dropped even more up to a factor of 100. The reduction of the C emission with each subsequent boronization is not so pronounced.

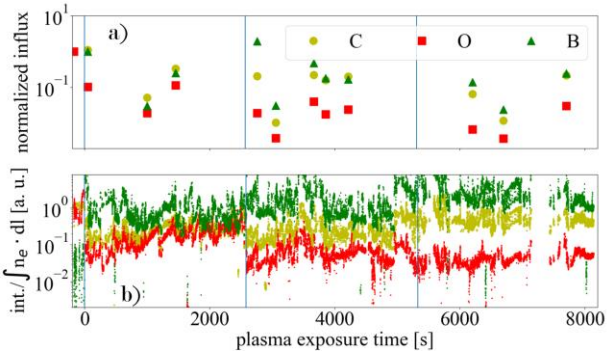

Figure 11: Time evolution of the main low Z impurities O and C as well as B: a) normalized influx, b) intensity of OVI, CVI and BV lines normalized to the line integrated density. The values are plotted as a function of the total plasma exposure time in all magnetic configurations normalized by the values before boronization. The vertical blue lines show boronization occurrences.

Photon fluxes of CIII (465.4 nm) and OII (441.9 nm) lines at the stainless steel wall show qualitatively the same behaviour as shown in Figure 12. The conversion of photon fluxes to impurity fluxes is rather complicated in this case since no diagnostics are available at these locations to provide T_e and n_e.
The results of mass spectrometry complement the spectroscopical data showing that partial pressure of CO and CO_2 decreased by a factor of 8 and 12 correspondingly (Figure 13). A reduction in H_2O content was also recorded, approximately by a factor of 2. There was no change in CH_4 pressure in the outgassing phase immediately after the first boronization.

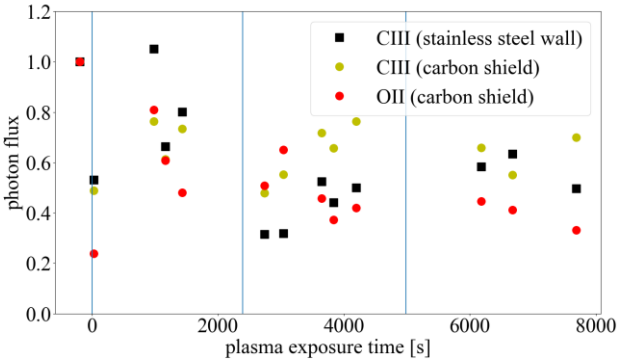

Figure 12: Time evolution of CIII (465.4 nm) and OII (441.9 nm) photon flux obtained with the filterscope system normalized to the values before boronization as a function of total plasma exposure time.

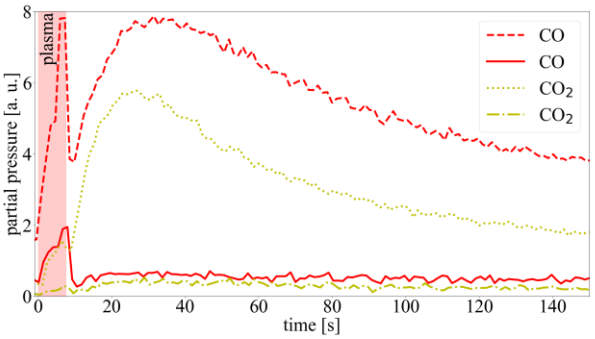

Figure 13: Mass spectrometry results for CO and CO_2 before (20180801.021) and after (20180807.011) boronization.

This implies that the main mechanism of C erosion before boronization was via formation of CO and CO_2 at the divertor. After the boronization O levels significantly dropped due to its gettering by B. The main zone of gettering is the recessed PFCs, since B is quickly eroded at the strike line location. Additional mechanisms such as reduced chemical erosion of C by H due to a:B/C-H layer [5] play smaller role and could not be quantified due to undetectable radiation of corresponding molecular bands at the divertor.
With every subsequent boronization O levels were decreasing even further due to the appearance of new B layers and, therefore, free B atoms which getter O via oxides formation.

5. Morphology and chemical composition

Interpretation of post-mortem analysis of the plasma-facing components is rather complicated due to the complex 3D nature of plasma-wall interaction in W7-X. Erosion zones at the divertor target plates give no information about deposited boron layers during boronizations. In contrast, the re-deposition zones can provide information about chemical composition of the a-B/C:H layers because of boronizations and the a-C:H layer due to natural deposition during plasma discharges.

Figure 14a is a scanning electron microscope image of a focused ion beam (FIB) cross-section of such a region. The blue line is the axis along which plots in Figure 14b were plotted. Figure 14b shows concentration profiles of carbon, oxygen, boron and iron profiles of a re-deposition zone at the divertor target (the location of the sample is shown in Figure 3 in orange) obtained with energy-dispersive X-ray spectroscopy (EDX).

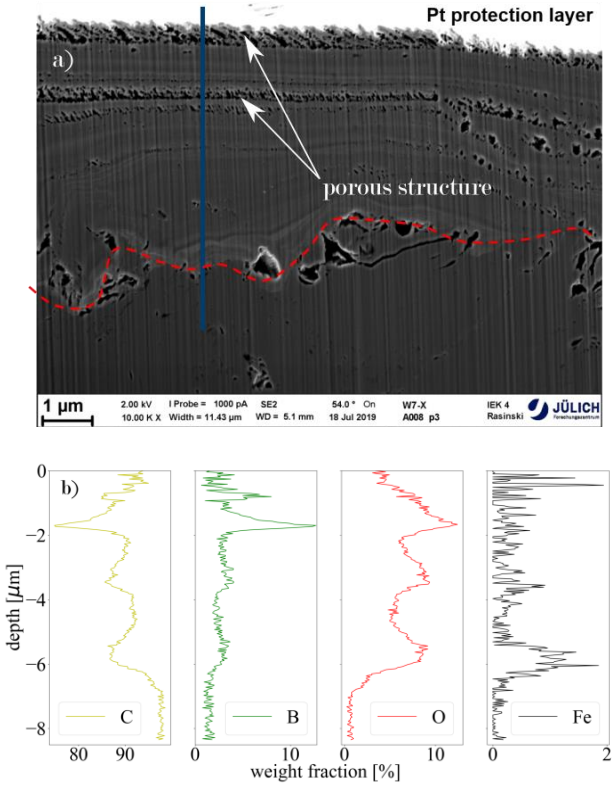

Figure 14: a) Scanning electron microscope (SEM) image of a re-deposition zone on the TM2h6 A008 element of the divertor (its location is shown in orange in Figure 3), blue line is the axis of the EDX scan. The red dashed line corresponds to the interface between the graphite tile and the re-deposited layer; b) Concentration profiles of carbon, oxygen, boron and iron.

The concentration profile of oxygen show 3 distinctive peaks and the corresponding profile of carbon clearly shows 3 distinctive drops, which can be related to the 3 boronizations of the campaign. Simultaneously, the boron profile shows a clear peak for the third boronization, but for the first two boronizations the peaks are less pronounced. This gives another argument that the oxygen and boron peaks are due to the boronizations and not due to re-deposition. Similar behaviour of both curves gives another evidence that oxygen is gettered by boron oxide formation.

These results show that in addition to the free B introduced with boronizations another mechanism plays a significant role to provide newly available B atoms: erosion and re-deposition.

Iron shows a peak at -6 µm in the FIB cross-section, which is related to the He glow-discharge cleaning performed frequently before boronization. During these discharges iron was eroded from the metal components by He ion impact on the steel and transported to these deposition zones.

Another interesting point is the porous structure at -2 µm in the FIB cross-section and on the top of the sample. The position of this structure correlates with the application of He-ECWC, but to make a conclusion a more deep investigation would be required. With the new divertor manipulator [26] available in the next operation phases it will become possible to introduce material samples to investigate this assumption in detail.

Summary and discussion:

A boronization has been applied for the first time at the Wendelstein 7-X stellarator. As a result the plasma-facing components have been covered with a protective boron layer. It has significantly widened the operational window of the device in terms of line-integrated density (from $4 \cdot 10^{19}$ m^{-2} up to $10 \cdot 10^{19}$ m^{-2}) and diamagnetic energy (from 330 kJ to 510 kJ). Z_{eff} values decreased from high values of 4.5 down to values close to 1.2 as was seen from bremsstrahlung measurements. The above given values were obtained in the two reference discharges with the same heating and fueling scenario before and after boronization.

Such an improvement became possible due to the substantially reduced content of the low-Z impurity O in the plasma: by a factor of 10 after the first boronization and by a factor of 100 after the third one. This improvement with the subsequent boronizations was caused by the increased coverage of PFCs as well as finite source of oxygen in the device. In its turn, this reduction has lead to decrease in the second low-Z impurity C. It was found that the chemical erosion of C by O was the main source of molecular impurities,

such as CO and CO_2 before boronization, as shown by mass spectroscopy.
After boronization the chemical erosion of C by O was strongly suppressed. The beneficial effect of the boronization has not deteriorated even after the protective boron layer was eroded at the strike line location on the divertor. This finding supports the assumption that the main effect of boronization was the gettering of oxygen on the recessed wall areas. Both low impurity concentration and the lifetime of PFCs are important questions for the future operation phase of W7-X, which aims for steady-state discharges of duration up-to 1800 s. A newly installed actively cooled divertor and other components will require a new set of boronizations. Such a long discharge is equivalent to the duration of all plasma discharges between boronizations in OP1.2 and will be performed in one magnetic configuration. It means that at the beginning of a discharge the newly deposited boron layer will be quickly eroded and the erosion and re-deposition mechanism will quickly saturate creation of newly present B atoms. Together with C erosion at the strike line, its transport to the remote areas, an increase of temperature of PFCs with increased water release bring a challenge for this phase.

Acknowledgements:

This work has been carried out within the framework of the Eurofusion Consortium and has received funding from the Euratom research and training programme 2014-2018 and 2019-2020 under grant agreement No. 633053. The views and opinions expressed herein do not necessarily reflect those of the European Commission.

References:

[1] J. Winter et al., 1989 Journal of Nuclear Materials 162-164
[2] T. Sunn Pedersen et al., 2019 Nucl. Fusion 59 096014
[3] R. König et al., 2004 Fusion Science and Technology 46
[4] U. Schneider et al., 1992 Fusion Technology 376-380
[5] J. Winter, 1996 Plasma Phys. Control Fusion 38 1503-1542
[6] P. Wienhold et al., 1992 Journal of Nuclear Materials 196-198 647-652
[7] A. Refke et al., 1994 Journal of Nuclear Materials 212-215 1255-1259
[8] T. Wauters et al., 2018 Nuclear Mat. and Energy 17 235-241
[9] A. Goriaev et al., 2019 submitted to Physica Scripta
[10] S. Brezinsek et al., 2005 Journal of Nuclear Materials 337-339 1058-1063
[11] U. Schneider et al., 1990 Journal of Nuclear Materials 176&177 350-356
[12] K. Nishimura et al., 2003 J. Plasma Fusion Res. 79 1216-1217
[13] E. Gaunthier et al., 1992 Jouranl of Nuclear Materials 196-198 637-641
[14] G. Jackson et al., 1992 Jouranl of Nuclear Materials 196-198 236-240
[15] S. Sudo et al., 1990 Nuclear Fusion 30 11
[16] Y. Wei et al., 2018 AIP Advances 8 085011
[17] Y. Liang et al., 2017 Nuclear Fusion 57 066049
[18] O. Neubauer et al., 2019 Fusion Engineering and Design 146 19-22
[19] R. Laube et al., 2011 Fusion Engineering and design 86 1133-1136
[20] L. Stephey et al., 2016 Rev. of Sci. Instr. 87 11D606
[21] http://open.adas.ac.uk/
[22] S. Brezinsek et al., 2011 Journal of Nuclear Materials 417 624-628
[23] D. Zhang et al., 2010 Rev. of Sci. Instr. 81 10E134
[24] G. Fuchert et al., 2020 Nucl. Fusion 60 036020
[25] D. Zhang et al., 2019 Phys. Rev. Lett 123 025002
[26] M. Hubeny et al., 2019 Nuclear Mat. and Energy 18 77-81